Grain Boundary Engineering to Control the Intergranular Stress Corrosion Cracking of Pipeline Steel

M.A. Arafin,[1] J.A. Szpunar[1]
[1] *McGill University, Montreal, Canada*

Abstract: The roles of grain boundary character and crystallographic texture on intergranular stress corrosion cracking (IGSCC) of API-X65 pipeline steel have been studied using Electron Backscattered Diffraction (EBSD) and X-Ray texture measurements with an ultimate objective to engineer the structure of grain boundaries to avoid such cracking.

It has been found that low-angle and special coincident site lattice (CSL) boundaries (mainly, Σ11 and Σ13b) are crack-resistant while the random high-angle boundaries are prone to cracking. However, several cracks were found to have been arrested even when random high-angle boundaries were available for them to continue propagating. Texture analyses revealed that {110}//RP and {111}//RP textured grains, mainly associated with <110> and <111> boundary rotation axes, respectively, were dominant in the vicinities of these crack-arrest points while the cracked boundaries were mainly linked to the {100}//RP textured grains. Controlled thermo-mechanical treatment could be utilized to produce these crack-resistant boundaries.

1. Introduction:

Stress corrosion cracking (SCC), both intergranular (IGSCC) and transgranular (TGSCC) types, is one of the major causes of pipeline failure throughout the world [see e.g. 1-3]. Despite the fact that the intergranular kind of SCC in pipeline steels was discovered long earlier than its transgranular alternative and has been extensively studied in the literature, the structural characteristics of these steels that are conducive or resistant to such cracking still remained unexplored.

Since IGSCC follows the grain boundary path, identifying the crack-resistant boundaries is of paramount importance. Random high angle grain boundaries (HAB) are known to provide easy crack propagation path due to their high energy configurations, while the low angle (LAB) and special coincidence site lattice (CSL) boundaries have the opposite characteristics [4,5]. The previous studies on the role of grain boundary to IGSCC in austenitic alloys showed that the special CSL boundaries were *mainly twins* (Σ3), while the other types of CSL boundaries were not immune to cracking [6,7]. The API X65 pipeline steel is ferritic-pearlitic which do not exhibit noticeable twinning; however, Venegas et al. [8] found that Σ11, Σ13b, and Σ29a CSL boundaries could be considered special in API X46 pipeline steel because they were resistant to intergranular hydrogen induced cracking (HIC). It is not clear, however, that whether these boundaries are special in providing resistance to IGSCC in this steel, not to mention the API X65 steels.

Several studies in the literature suggest that texture plays a key role in the different types of cracking process [see e.g. 8-16]. But, unfortunately, no such

studies were found in the literature that evaluated the role of crystallographic texture in the intergranular stress corrosion cracking of pipeline steels except the one reported by Alexandreanu and Was [17]; but the inclusion of texture in that study was only limited to assessing whether the cracked boundaries belonged to the grains of similar or dissimilar orientations and, also, the material of their study was austenitic nickel-based (Ni-16Cr-9Fe) alloy which is not used in the pipeline industry. The authors concluded that, by comparing the Taylor Factors, boundaries associated with grains of dissimilar orientations are susceptible to cracking and the ones with similar orientations are less vulnerable. However, they did not identify any crack resistant boundaries associated with certain textured grains. It should be pointed out here that crystallographic orientations of the neighbouring grains determine the misorientation angle and axis of the boundary associated with them. It is also known that energy of grain boundaries is heavily dependent not only on the misorientation angle but also on the axis of rotation. In other words, for the same misorientation angle but different rotation axis, the boundary energy can be significantly different. The objective of this study is, therefore, to identify the special boundaries in API X-65 pipeline steel that can resist IGSCC and to examine whether crystallographic texture plays a key role in such cracking.

2. Experimental:

The API X65 test coupons were taken out from an in-service high-pressure natural gas transmission pipeline that experienced severe intergranular stress corrosion cracking. The wall-thickness of the pipe was approximately 1 cm.

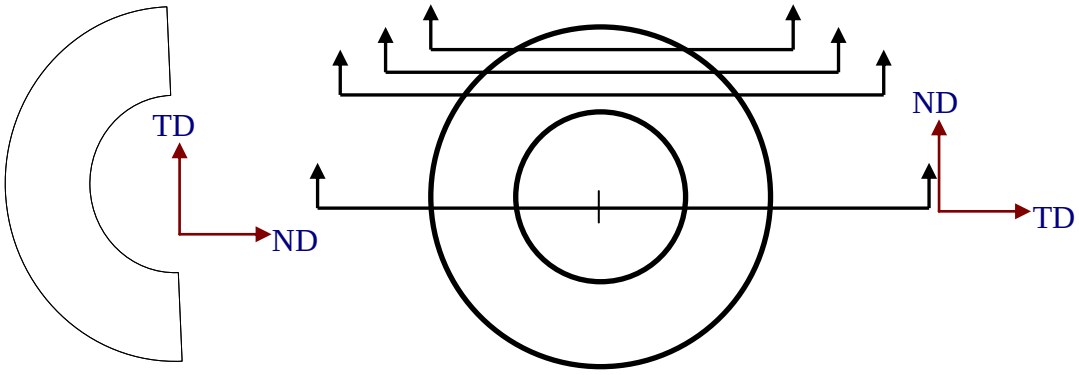

Fig. 1 Sample preparation for macro- and microtexture studies

The samples were cut along the TD-ND section (see Fig. 1) to study the grain boundary character distribution (*GBCD)* and microtexture in order to identify the characteristics of the grain boundaries and texture that are susceptible to IGSCC and the ones that resist such cracking. Microtexture and Mesotexture studies were conducted using Philips XL30S FEG SEM equipped with EBSD detector and TSL OIM Analysis Software. X-Ray macrotexture measurements

were carried out at different layers of the pipe thickness along the RD-TD sections to study the non-homogeneity of texture and grain boundary misorientation distributions through the thickness. The X-Ray texture studies were carried out using the Siemens D-500 X-Ray Goniometer and the recorded experimental texture data were analyzed using the TexTools Software [18].

3. Results and Discussions:

3.1 Grain Boundary Character Distribution:

The grain boundary character distributions were obtained from several EBSD measurements along the pipe thickness. It was found (see Fig. 2) that HAB were more dominant in the pipe surface area which gradually decreased with the depth. On the other hand, LAB and CSL boundaries showed the opposite trend.

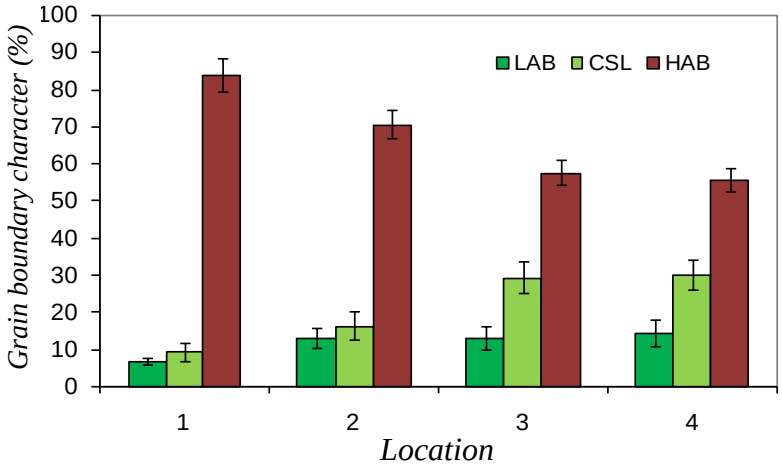

Fig. 2 GBCD variations along the pipe-thickness (locations 1, 2, 3 and 4 are 250 μm, 1.1 mm, 1.5 mm and 2 mm from the outer surface of the pipe, respectively)

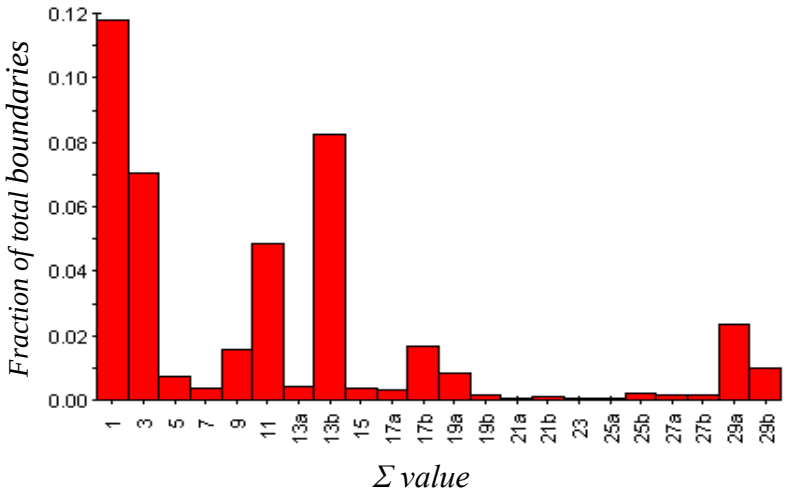

Fig. 3 Example of CSL boundary distribution in the crack-tip region

It is important to note that the CSL boundaries, other than Σ1 which are essentially low angle boundaries, found in the crack-tip regions were mainly $\Sigma 3^n$, Σ11 and Σ13b types, as shown in Fig. 3. However, true twinning/multiple twining does not occur in low-carbon steels [8] and, hence, $\Sigma 3^n$ boundaries cannot be considered special that resist cracking. Therefore, Σ11 and Σ13b are the only ones that might be considered as special because they had a strong presence in the regions just beyond the crack-tips.

3.2 Role of Grain Boundary Character on Crack Propagation and Arrest:

Figures 4a and 4b show two examples of EBSD image quality maps in which the grain boundaries were identified along the crack propagation paths and at the crack-arrest points. The cracked boundaries were all found to be random high angle boundaries. It should be noted here that hoop stress was acting on the y (vertical)-direction and, therefore, the horizontal boundaries were the most susceptible. However, the cracks got deflected on several instances when the crack-front met any crack-resistant boundaries that were favourably oriented with respect to the stress axis. The special crack-resistant boundaries were mainly found to be LAB, Σ11 and Σ13b which is consistent with the observations reported in section 3.1. An important point to note here that occasionally crack back-turn, i.e. boundary inclination was more than 90° with respect to the forward horizontal direction, was observed (see in both Figs. 4a and 4b) along the crack propagation path when the favourably oriented boundary ahead of the triple junction was a special boundary but the other, although unfavourably oriented, was a random high angle boundary. However, no back-turn was observed when at least one favourably oriented random high angle boundary was available for the crack-tip to continue propagating. This observation is of great significance to modeling studies of IGSCC because often such back-turn is either neglected [19] or always allowed [20]. The cracks got arrested in the triple junctions when both boundaries ahead of the crack-tip were special boundaries (see e.g. the crack-arrest point of the lower crack in Fig. 4a). One exception is shown in Fig. 4b where the triple junction at which the crack got arrested had a low-angle boundary ahead of the crack-tip, but a random high-angle boundary was available for the crack to continue propagating. This seemed to be quite unusual according to the conventional understanding of grain boundary characteristics. An important point to note here is that the grains associated with this boundary had orientations close to {110}//Rolling Plane (RP) with <110> boundary rotation axis. A variation of this type of crack-arrest point can be observed in the upper right hand corner of Fig. 4a. Like the previous example, one of the boundaries in front of this crack-arrest site was a favourably oriented random high angle boundary, but in this case, the crystallographic orientations of the two grains that shared this specific boundary were random as well. Detail investigations of this type of crack-arrest is reported in the next section.

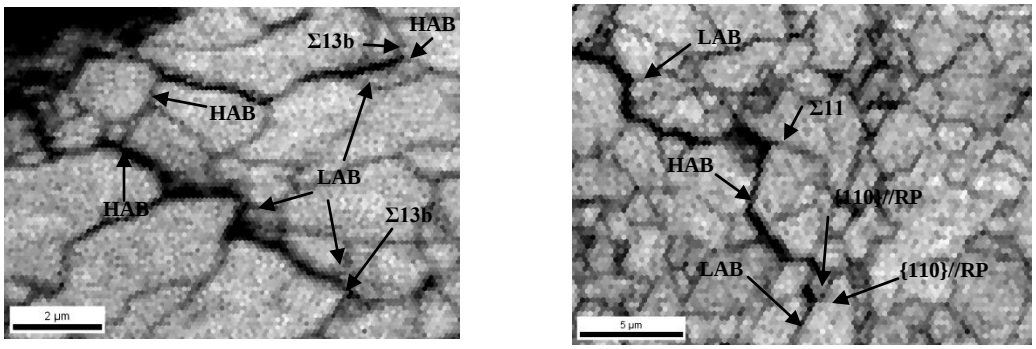

(a) *(b)*

Fig. 4 Grain Boundary Character analyses for crack propagation and arrest

3.3 Role of Texture on IGSCC - Microtexture Studies:

Contrary to the customary perception of grain boundary characteristics, several cracks were found to have been arrested in the triple junctions where a random high angle and favourably oriented boundary was available for the crack to continue propagating, as mentioned with examples in section 3.2. This also has far-reaching implication in a sense that it is not always the LAB and CSL boundaries at the triple point that can bring the crack to an arrest; there might be some other types of boundaries that can stop the crack propagation as well. Observation of this phenomenon has directed us to examine whether the crystallographic texture played a role in arresting these cracks.

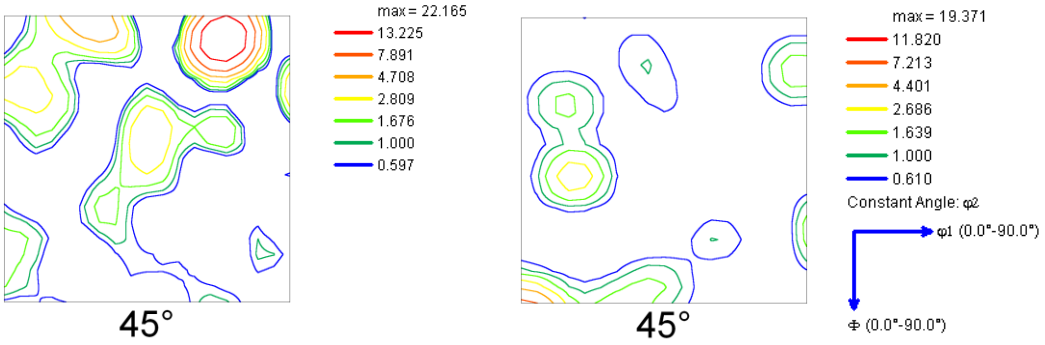

(a) *(b)*

Fig.5 φ_2 = 45° cross-section of ODFs of the pipeline steel along the (a) cracked and (b) immediately ahead of the crack-tip areas

ODFs (Orientation distribution functions) at φ_2 = 45° constant cross section have been calculated along the *crack path* and *just beyond the crack-tip regions*. As can be seen, from Fig. 5a, {001}//RP has the highest intensity along the crack propagation path suggesting that cracked boundaries are mainly linked to {100}//RP textured grains. On the other hand, Fig. 5b shows that {110}//RP was dominant in the latter case. In many instances, however, {111}//RP texture

was also observed, e.g. see Fig. 6, in the locations immediately ahead of the crack-arrest sites. A number of crack-arrest points and the regions just beyond these locations showed similar behaviour indicating that boundaries associated with {110}//RP and {111}//RP textured grains are resistant to cracking and, when several {110}//RP and {111}//RP textured grains are clustered together in a region, they can effectively enhance the IGSCC resistance of that area that might include few neighbouring grains in the vicinity of the cluster as well which can be thought of as extended zone-effect. This is analogous to the "toughening/ductilization of brittle materials" by incorporating several low energy boundaries in the form of clusters, as proposed by Watanabe [21] and, therefore, suggests that grain boundaries linked to the {110}//RP and {111}//RP textured grains have low energy configurations which will be discussed further in section 3.5. It is worth mentioning here that Σ11 and Σ13b boundaries are also defined with <110>/50.48° and <111>/27.8° rotation axes-angle [22], respectively, the fractions of which could be significantly increased by the {110}//RP and {111}//RP textured grains.

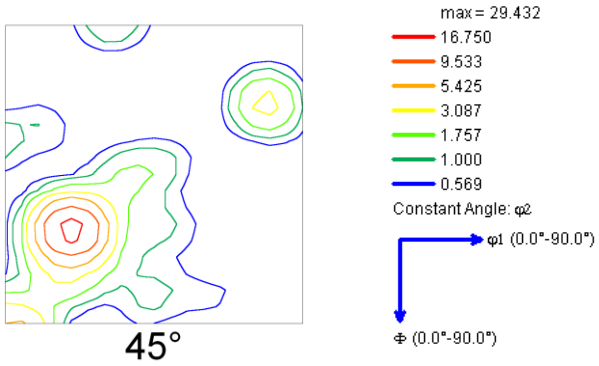

Fig.6 φ_2 = 45° cross-section of ODFs immediately ahead of the crack-tip area showing the dominant {111}//RP texture

3.4 Macrotexture Studies through the Pipe-thickness:

X-ray texture studies have been carried out on a *non-cracked sample* of the same pipe in order to further verify the observations obtained from the EBSD data. The obtained grain boundary character distribution from the X-ray texture data suggests that the high angle grain boundaries are dominant at the pipe surface and did not decrease significantly with depth, as shown in Fig. 7. However, no cracks were found to have been initiated in this sample except some small corrosion pits on the surface layer.

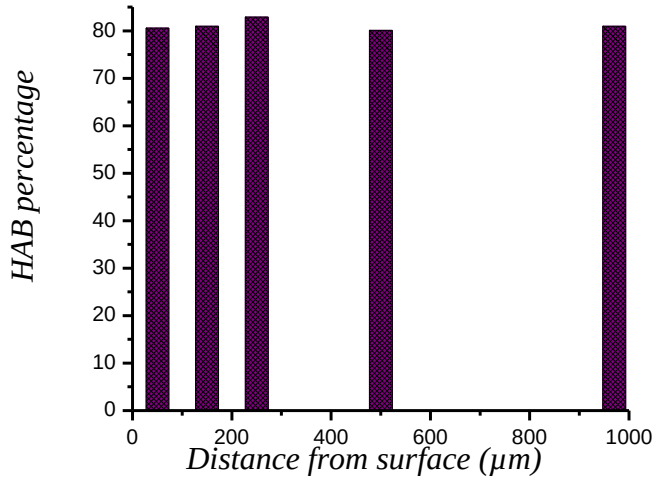

Fig. 7 HAGB percentage through the pipe thickness

ODF at φ_2 = *45° section* showed that {100}//RP texture was very weak (approximately 0.5 times the random intensity) at the surface, however the {110}//RP texture had the highest intensity along with the {111}//RP fiber, as shown in Fig. 8.

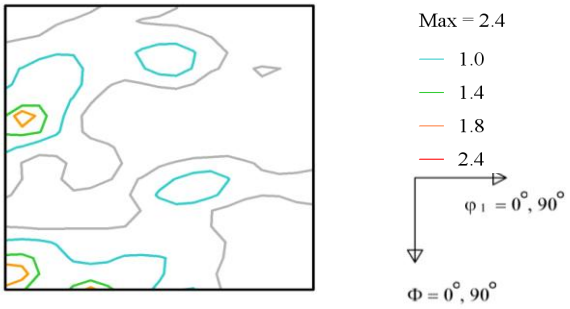

Fig. 8 ODF at φ_2 = 45° section at a depth of 150 μm from the surface

It should be noted here that intensities of the ODFs obtained from the EBSD scan data, for the cracked and immediately ahead of the crack-tip regions, and X-ray texture measurements must not be compared. EBSD results represent very local textures, while the macroscopic texture data were obtained from the X-ray texture measurements with 2.2 cm x 1.3 cm specimens. The intensity data indicates that {110}//RP and {111}//RP textures have five times and three times higher intensities, respectively, than the {100}//RP texture in the non-cracked sample. This supports the previous observations that {110}//RP and {111}//RP textures could resist the crack propagation.

Therefore, it can be concluded that the intergranular stress corrosion cracks can be arrested either by incorporating high fraction of LAB and special CSL boundaries or, by creating {110}//RP and {111}//RP textures close to the pipe surface.

3.5 Crack Propagation Resistance for {110}//RP and {111}//RP Textured Steels:

The possible explanation of the observation that {110}//RP and {111}//RP textures are resistant to intergranular fracture is that, in steel, <110> and <111> misorientation axes (both for tilt and twist type boundaries), associated with the {110}//RP and {111}//RP grains, have lower grain boundary energies than the ones with <100> misorientation axis associated with the {100}//RP textured grains [23]. This is true for both low and high angle boundaries. Similar calculations, although for low angle boundaries only, were also presented by Yang et al. [24]. The axis/angle misorientation distribution in the crack-arrest regions, an example is shown in Fig. 9, indeed revealed that the rotation axes of these grain boundaries were mainly <110> and <111>. This, again, justifies the conclusion that boundaries associated with {110}//RP and {111}//RP textured grains are more likely to resist crack propagation.

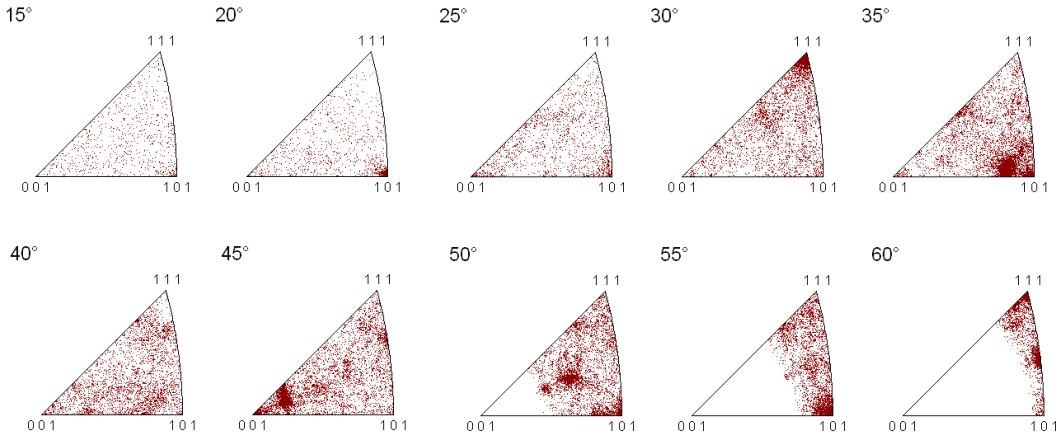

Fig. 9 Example of axis/angle distribution in the crack-arrest region

4. Conclusions:

Following conclusions can be made from the above study:

1. Low angle and special CSL boundaries (mainly of Σ11 and Σ13b types) are resistant to intergranular stress corrosion cracking in API X65 pipeline steel while the random high angle grain boundaries are susceptible to such cracking
2. Crystallographic texture affects the intergranular stress corrosion cracking of pipeline steel. Grain boundaries associated with the {110}//RP and {111}//RP textured grains provide high resistance to IGSCC whereas, the boundaries of {100}//RP textured grains are the most vulnerable.

3. IGSCC initiates at the pipe outer surface and, therefore, could be avoided either by providing a large fraction of low-angle and special CSL boundaries that can be incorporated by appropriate grain boundary engineering methods such as controlled thermo-mechanical treatments or, by modifying the crystallographic texture in this region.

References:

[1] Federal Power Commission, Bureau of Natural Gas, Washington DC. Final staff report on investigation of Tennessee Gas Transmission Company Pipeline No 100-1 failure near Natchitoches, Louisiana, March 4, 1965, Docket No. CP65-267

[2] P.J. Kentish, Gas pipeline failures: Australian experience, Br Corros J 20 (1985) 139-146

[3] National Energy Board (NEB) Report (1996); Public Inquiry Concerning Stress Corrosion Cracking on Canadian Oil and Gas Pipelines, MH-2-95

[4] T. Watanabe, An approach to grain boundary design for strong and ductile materials, Res Mechanica 11 (1984) 47-84

[5] D.C. Crawford, G.S. Was, The role of grain boundary misorientations in intergranular cracking of Ni-16Cr-9Fe in 360°C argon and high purity water, Metall Mater Trans A 23 (1992) 1195-1206

[6] H. Lin, D.P. Pope, The influence of grain boundary geometry on intergranular crack propagation in Ni3Al, Acta Metall Mater 41 (1993) 553-562

[7] V.Y. Gertsman, S.M. Bruemmer, Study of grain boundary character along intergranular stress corrosion crack paths in austenitic alloys, Acta Mater 49 (2001) 1589-1598

[8] V. Venegas, F. Caleyo, J.M. Hallen, T. Baudin, R. Penelle, Role of crystallographic texture in hydrogen-induced cracking of low carbon steels for sour service piping, Metall Mater Trans A 38 (2007) 1022-1031

[9] C.J. Taylor, T. Zhai, A.J. Wilkinson, J.W. Martin, Influence of grain orientations on the initiation of fatigue damage in an Al-Li alloy, J Microsc 195 (1999) 239-247

[10] M. Mineur, P. Villechaise, J. Mendez, Influence of the crystalline texture on the fatigue behavior of a 316L austenitic stainless steel, Mater Sci Eng A 286 (2000) 257-268

[11] T. Zhai, A.J. Wilkinson, J.W. Martin, The effects of micro-texture and β' particle distribution on short fatigue crack growth in an Al-Li 8090 alloy, Mater Sci Forum 331-337 (2000) 1549-1554

[12] J.I. Verdeja, J. Asensio, J.A. Pero-Sanz, Texture, formability, lamellar tearing and HIC susceptibility of ferritic and low carbon HSLA steels, Mater. Charact. 50 (2003) 81-86

[13] U. Krupp, O. Duber, H.J. Christ, B. Kunkler, A. Schick, C.P. Fritzen, Application of the EBSD technique to describe the initiation and growth behavior of microstructurally short fatigue cracks in a duplex steel, J Microsc 213 (2004) 313-320

[14] K. Shimizu, T. Torii, The effect of microstructure evaluated by electron backscatter diffraction method on fatigue crack propagation behavior in rolled copper film, Fatigue Fract Eng Mater Struct 28 (2005) 221-227
[15] A. Boumaiza, T. Baudin, N. Rouag, R. Penelle, Electron backscattered diffraction of transgranular crack propagation in soft steel, Chin Phys Lett 24 (2007) 1759-1762
[16] H. Koh, T. Sakai, H. Utsunomiya, S. Miamiguchi, Deformation and texture evolution during high-speed rolling of AZ 31 magnesium sheet, Mater Trans 48 (2007) 2023-2027
[17] B. Alexandreanu, G.S. Was, The role of stress in the efficacy of coincident site lattice boundaries in improving creep and stress corrosion cracking, Scripta Mater 54 (2006) 1047-1052
[18] TexTools Software, Resmat Corporation, Montreal, QC, Canada
[19] Y. Pan, T. Olson, B.L. Adams, Applications of orientation imaging analysis to microstructural control of intergranular stress corrosion cracking, Can Metall Q 34 (1995) 147-154
[20] V.Y. Gertsman, K. Tangri, Modelling of intergranular damage propagation, Acta Mater, 45 (1997) 4107-4116
[21] T. Watanabe, Toward grain boundary design and control for advanced materials, in: U. Erb, G. Palumbo (Eds.) Grain Boundary Engineering, Canadian Institute of Mining, Metallurgy and Petroleum, Montreal, QC, 1993, pp. 57-87
[22] H. Mykura, A checklist of cubic coincidence site lattice relations, in: Grain Boundary Structure and Kinetics, ASM Materials Science Seminar, ASM International, Materials Park, OH, 1980, pp. 445-456
[23] Y. Hayakawa, J.A. Szpunar, The role of grain boundary character distribution in secondary recrystallization of electrical steels, Acta Mater 45 (1997) 1285-1295
[24] C.C. Yang, A.D. Rollett, W.W. Mullins, Measuring relative grain boundary energies and mobilities in an aluminum foil from triple junction geometry, Scripta Mater 44 (2001) 2735-2740